Journal of Materials Chemistry A

ROYAL SOCIETY OF CHEMISTRY

PAPER

View Article Online
View Journal | View Issue

Published on 07 May 2020. Downloaded by University of Technology Sydney on 08/19/2020 15:34:40.

Check for updates

Cite this: J. Mater. Chem. A, 2020, 8, 15884

Surface-functionalized palladium catalysts for electrochemical CO_2 reduction†

Rong Xia,[ab] Sheng Zhang,*[a] Xinbin Ma[a] and Feng Jiao*[b]

Received 27th March 2020
Accepted 7th May 2020

DOI: 10.1039/d0ta03427d

rsc.li/materials-a

Rational design and synthesis of efficient catalysts for electrochemical CO_2 reduction is a critical step towards practical CO_2 electrolyzer systems. In this work, we report a strategy to tune the catalytic property of a metallic Pd catalyst by coating its surface with a polydiallyldimethyl ammonium (PDDA) polymer layer. The resulting PDDA-functionalized Pd/C catalysts exhibit an enhanced CO faradaic efficiency of ~93% together with a current density of 300 mA cm^{-2} at −0.65 V *versus* reversible hydrogen electrode in comparison to non-functionalized and commercial Pd/C catalysts. X-ray photoelectron spectroscopy analysis reveals that the improvement can be attributed to the electron transfer from the quaternary ammonium groups of PDDA to Pd nanoparticles, weakening the CO binding energy on Pd. The weak CO adsorption on Pd was further confirmed by the CO temperature programmed desorption measurement and operando attenuated total reflection-Fourier-transform infrared analysis. Therefore, the incorporation of electron-donating groups could be an effective strategy to decrease the CO binding energy of a metallic catalyst for a high CO selectivity in CO_2 electroreduction.

1. Introduction

Electrochemical CO_2 reduction (CO_2R) has been investigated as a potential route to utilize CO_2 as the carbon feedstock for fuel and chemical production. Coupling with renewable electricity generation, this approach provides an alternative approach to replace conventional petroleum-based processes. Numerous works have been dedicated to developing efficient CO-selective metal catalysts, such as Au,[1–3] Ag,[4–6] Zn,[7,8] and Pd.[9–12] Among them, Pd exhibits distinct electrocatalytic properties under different overpotential regions in CO_2R. In neutral electrolytes, formate is the dominant CO_2R product on Pd catalysts at low overpotentials, whereas CO becomes the main product at high overpotentials (lower than −0.5 V *versus* reversible hydrogen electrode, RHE). The shift of product selectivity is probably due to the formation of Pd hydride phase at high overpotentials, which alters the CO_2R mechanism on the catalyst surface.[13,14] As high current densities are generally required for commercial electrolysis systems, Pd catalysts are likely operated under the CO-selective potential region, *i.e.*, relatively high overpotentials. More efforts are needed to further reduce the required overpotential for Pd-based catalysts.

In theory, a metal catalyst with a weak CO binding energy should exhibit a high CO selectivity in CO_2R because of the facile desorption of the CO intermediate from the catalyst surface. Weakening the CO binding strength on Pd surface could be an effective strategy to improve CO selectivity while maintaining a low overpotential for CO_2R. Many efforts have been devoted into tuning CO binding energy of Pd catalysts by changing the surface strains,[15,16] controlling the morphologies and nanostructures,[17–19] and alloying with a second metal.[20–22] Recently, Sargent *et al.* reported a molecular tuning strategy by functionalizing metal catalyst surface with organic molecules, which are specifically designed to stabilize reaction intermediates for improved performances.[23] This strategy could be also applied to modify the electronic structure of Pd surface by incorporating a molecular layer with desired functional groups, which can potentially enhance CO selectivity in CO_2R at low overpotentials.

Polydiallyldimethyl-ammonium chloride (PDDA) has been employed to functionalize Pt nanocatalysts. Because of the surface interactions, PDDA not only immobilizes Pt nanoparticles on the carbon support, but also increases Pt oxidation potential in oxygen reduction reaction.[24] Here, we reported a molecular functionalization method in which PDDA was coated on the surface of Pd nanoparticles as a means to tune the CO adsorption strength of Pd catalysts. The PDDA-functionalized Pd/C catalysts show a maximum current density of 300 mA cm^{-2} together with a CO faradaic efficiency (FE) of 93% in 1 M KOH electrolyte at −0.65 V *vs.* RHE. The

[a]Key Laboratory for Green Chemical Technology of Ministry of Education, Collaborative Innovation Center of Chemical Science and Engineering, School of Chemical Engineering and Technology, Tianjin University, Tianjin 300072, China. E-mail: sheng.zhang@tju.edu.cn

[b]Center for Catalytic Science and Technology, Department of Chemical and Biomolecular Engineering, University of Delaware, Newark, Delaware 19716, USA. E-mail: jiao@udel.edu

† Electronic supplementary information (ESI) available. See DOI: 10.1039/d0ta03427d

This journal is © The Royal Society of Chemistry 2020

Published on 07 May 2020. Downloaded by University of Technology Sydney on 08/19/2020 15:34:40.

overpotential for PDDA-functionalized Pd/C catalyst is significantly lower than what is needed for commercial and bare Pd/C catalysts. The originality of the performance enhancement was investigated using temperature programmed desorption (TPD) and operando attenuated total reflection Fourier-transform infrared spectroscopy (ATR-FTIR), both of which show a weakened CO binding strength on the Pd surface through the PDDA functionalization.

2. Experimental

2.1. Materials

Polydiallyldimethylammonium chloride (PDDA) (20%, average MW < 100 000) and potassium tetrachloropalladate (K_2PdCl_4, 99.99%) were obtained from Sigma-Aldrich. Potassium hydroxide (KOH, 99.99%) and sodium hydroxide (NaOH, 98%) were purchased from Aladdin. Carbon support (Vulcan XC-72R) was bought from the Fuel Cell Store. Sodium borohydride ($NaBH_4$, 98%) and isopropanol (IPA, 99.5%) were purchased from Technology Development Co., Ltd. Carbon fiber paper (TGP-H-060) was manufactured by Toray Industries, Inc. All chemicals were used without further purification.

2.2. Catalyst preparation

The synthetic method is adapted from a previous report.[24] For a typical synthesis of the PDDA-functionalized Pd/C catalysts, the precursor K_2PdCl_4 (61 mg) was first dissolved in 200 mL deionized water and then a solution of 20 wt% PDDA was added. To study the PDDA effect, four sets of samples were prepared by changing the mass fraction of PDDA loading: 0% (Pd/C-PDDA-0), 10% (Pd/C-PDDA-10), 20% (Pd/C-PDDA-20) and 40% (Pd/C-PDDA-40). In a separate container, 80 mg of Vulcan XC-72R activated carbon was sonicated in the mixture solution of isopropanol (20 mL) and deionized water (20 mL) for 20 minutes. Both solutions were then mixed and stirred for another 10 minutes, followed by an addition of freshly prepared sodium borohydride solution (15 mg $NaBH_4$ dissolved in 5 mL H_2O). After the mixture was stirred for 48 hours, 2 g of NaOH was added to adjust the pH. After another 48 hours of stirring, the final mixture was filtrated, washed repeatedly with de-ionized water until no chloride ion can be detected, and dried at 80 °C in a vacuum oven for 3 hours. The as-synthesized catalysts are denotes as Pd/C-PDDA-*X*, where *X* represents the mass fraction of PDDA loading.

2.3. Characterizations

The Pd loading in each sample was confirmed using Inductively Coupled Plasma Optical Emission Spectroscopy (ICP-OES) where the sample was dissolved in a mixture of 6 mL HCl (30 wt%), 2 mL HNO_3 (70 wt%). The ICP-OES results are summarized in Table S1.† X-ray diffraction (XRD) patterns were obtained using a Rigaku/max-2500 diffractometer with Cu Kα radiation (40 kV, 200 mA). The diffraction pattern was collected between 10–90° (2θ) with a scan speed of 8° min^{-1}. The samples were also characterized by transmission electron microscopy (TEM) using a JEM-2100F microscope operated at an accelerating voltage of 200 kV.

Carbon monoxide temperature-programmed desorption coupled with mass spectrometry (CO-TPD-MS) was performed using a Micromeritics AutoChem 2910 equipped with a thermal conductivity detector (TCD). The sample (0.1 g) was loaded in a U-type tube reactor. Prior to CO temperature-programmed desorption process, the samples were purged at 200 °C for 60 minutes under Ar flow for eliminating water and impurities in samples. The catalyst was then cooled to room temperature under Ar gas at 20 °C min^{-1} ramp and treated with 4% CO/He gas for 1 h. Finally, the TPD measurement was conducted by heating the sample to 800 °C with a ramp of 10 °C min^{-1} in Ar for desorption.

Operando attenuated total reflection-Fourier-transform infrared (ATR-FTIR) was measured by a Thermo Scientific Nicolet iS50 FTIR Spectrometer at a spectral resolution of 4 cm^{-1}. The Pd/C catalyst was coated on Au film using following procedures: the desired amount of catalyst ink was pipetted and chemically deposited on the basal plane of a hemicylindrical Si prism with a metal loading of 50 μg cm^{-2}. The ink was allowed to be dried and rinsed with deionized water. The catalyst layer was immersed in CO-saturated 0.1 M KOH solution under a constant CO flow at a rate of 10 sccm. FTIR spectra were recorded at applied potentials from −0.40 V to −0.70 V *versus* reversible hydrogen electrode (RHE). The background is recorded at 0.20 V *vs.* RHE.

2.4. Electrochemical measurement

2.4.1. Electrode preparation. The as-prepared catalysts (10 mg) were dispersed in isopropanol (1 mL) and 10 μL Nafion ionomer solution (5 wt% in water). The mixture was sonicated for 30 minutes and dropcast onto a carbon diffusion layer (GDL). The active area of each electrode is 1 cm^2 and the catalyst loading of each electrode was controlled to 1.5 mg cm^{-2}.

2.4.2. Electrochemical test. The PDDA-functionalized Pd/C catalysts were investigated in a 3-compartment microfluidic flow cell (Fig. S1†), similar to the design in previous studies.[25,26] A 1 M KOH solution was used as both catholyte and anolyte. An anion exchange membrane (PTFE Supported Sustainion 37–50 Alkaline Exchange Membranes) was used to separate cathode and anode chambers. A graphite counter electrode was used together with a Hg/HgO reference electrode. All the potentials reported here were converted regarding reversible hydrogen electrode (RHE) with *iR* correction based on the following equation (eqn (1)):

$$E_{\mathrm{RHE}} = E_{\mathrm{Hg/HgO}} + E^{0}_{\mathrm{Hg/HgO}} + 0.0591 \times \mathrm{pH} + iR \qquad (1)$$

where *i* stands for the applied current and *R* is the measured resistance *via* electrochemical impedance spectroscopy with the ripple frequency from 10^5 to 0.1 Hz and measurement amplitude of 10 mV.

2.5. Product quantification

The gas products were analyzed using online gas chromatography (Shimadzu) equipped with a PN column (1 m) and a MS-13X column (2 m). H_2 and CO were quantified using

Published on 07 May 2020. Downloaded by University of Technology Sydney on 08/19/2020 15:34:40.

a thermal conductivity detector (TCD), while hydrocarbons (*e.g.*, C_2H_4 and C_2H_6) were detected using a flame ionization detector (FID). CO and CH_4 were quantified by a separate FID detector after passing through a methanizer. Liquid products were quantified using nuclear magnetic resonance spectroscopy (NMR). In a typical measurement, 500 μL of sample is mixed with 100 μL of dimethyl sulfoxide (DMSO) solution (25 ppm in D_2O), which is used as an internal standard, followed by the NMR analysis. The ^{1}H NMR spectra are analyzed with solvent presaturation implemented to suppress the water peak.

The faradaic efficiency (FE) for each product was calculated according to the following equations (eqn (2) and (3)):

$$\mathrm{FE}(\%) = \frac{Q_{\mathrm{Prod.}}}{Q_{\mathrm{Total}}} \times 100 = \frac{nFx\nu}{j_{\mathrm{tot}}} \times 100 \quad (2)$$

$$\mathrm{FE}(\%) = \frac{Q_{\mathrm{Prod.}}}{Q_{\mathrm{Total}}} \times 100 = \frac{nFcV}{Q} \times 100 \quad (3)$$

where n is the number of electrons transferred, F is the Faraday constant, x is the molar fraction of gas product determined by GC, ν is the gas flow rate (L s^{-1}), j_{tot} is the total current (A), c is the liquid product concentration (mol L^{-1}), V is the volume of liquid product (L) and Q is the total charge passed the electrode (C).

3. Results and discussion

A schematic representation of the synthetic approach of PDDA-functionalized Pd/C catalysts is shown in Fig. 1a. PDDA chains contain positively charged quaternary ammonium groups that

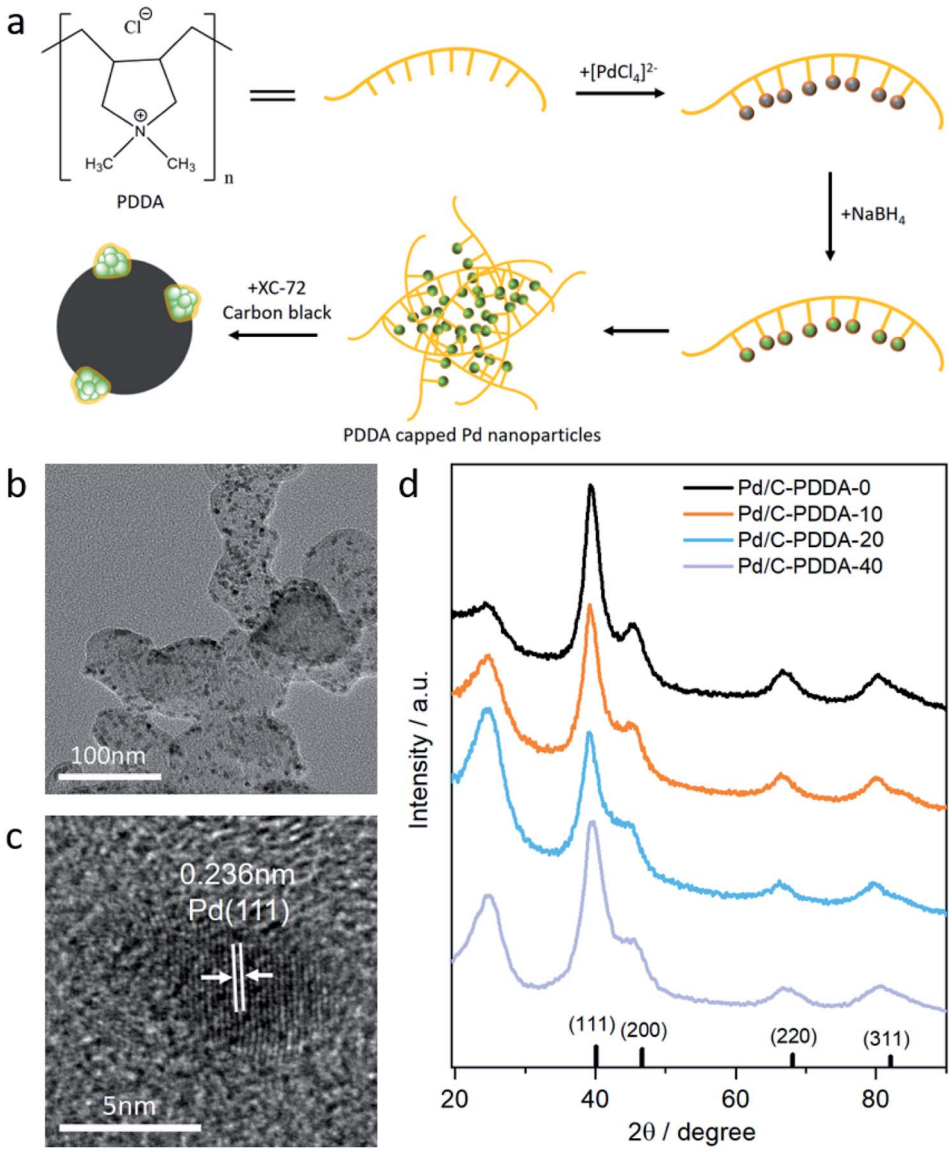

Fig. 1 (a) Schematic diagram of the synthesis of PDDA-functionalized Pd/C catalysts. Typical (b) TEM and (c) HRTEM images of the as-synthesized Pd/C-PDDA-20, and (d) XRD patterns of as-synthesized PDDA-functionalized Pd/C catalysts as well as the non-PDDA-functionalized Pd/C sample (Pd/C-PDDA-0).

 This journal is © The Royal Society of Chemistry 2020

Published on 07 May 2020. Downloaded by University of Technology Sydney on 08/19/2020 15:34:40.

interact with $[PdCl_4]^{2-}$ anions to ensure a homogeneous, uniform loading of the Pd precursors. Upon a chemical reduction by $NaBH_4$, metallic Pd nanoparticles are formed localled in close contact with the quaternary ammonium groups, which is critical for enhanced CO_2 electroreduction to CO. The addition of carbon black (XC-72) improves the dispersion of the PDDA-functionalized Pd particles.

Transition electron microscope (TEM) images of Pd/C-PDDA-*X* (Fig. 1b and S2†) show a uniform dispersion of Pd nanoparticles with a spherical shape on the carbon support across all samples. Based on the particle size distribution histograms (Fig. S2†), average sizes of 2.9, 3.0, 2.2, and 2.3 nm are estimated for Pd/C-PDDA-0, Pd/C-PDDA-10, Pd/C-PDDA-20, and Pd/C-PDDA-40, respectively. To evaluate the atomic structure of as-synthesized Pd/C-PDDA-*X*, both high-resolution TEM (HRTEM) and powder X-ray diffraction (XRD) measurements were conducted. Fig. 1c is a typical HRTEM image of Pd/C-PDDA-20, which shows a distance between two neighboring fringes of 0.236 nm, corresponding to the space of Pd(111) crystal planes. The crystal structure of Pd particles in the Pd/C-PDDA-*X* is further examined by XRD analysis. All the diffraction peaks (Fig. 1d) align well with the standard pattern of metallic Pd (JCPDS no. 46-1043), confirming that cubic metallic Pd nanoparticles are formed in all Pd/C-PDDA-*X*. Crystallinite sizes estimated from the diffraction patterns using the Scherrer formula (Table S2†) are 3.0, 2.9, 2.5, and 2.6 nm for Pd/C-PDDA-0, Pd/C-PDDA-10, Pd/C-PDDA-20, and Pd/C-PDDA-40, respectively, which are consistent with the values obtained from the TEM analysis (Fig. S3†).

The CO_2 electrocatalytic properties of Pd/C-PDDA-*X* catalysts were evaluated using a typical 3-compartment microfluidic cell configuration, similar to our previous work.[27,28] All potentials reported are converted to reversible hydrogen electrode (RHE) unless stated otherwise. The CO_2R results are summarized in Fig. 2, in which catalytic properties for commercial Pd/C are also measured for comparison. Among all the Pd/C-PDDA-*X* catalysts, Pd/C-PDDA-20 exhibited the highest current density (up to 300 mA cm^{-2}) together with a CO FE of ~93% at −0.65 V (Fig. 2a and b), which corresponds to a CO partial current density of ~279 mA cm^{-2}. Interestingly, both Pd/C-PDDA-10 and Pd/C-PDDA-40 show significantly lower performance than Pd/C-PDDA-20. At low PDDA loadings, the amount of PDDA may not be sufficient to interact with Pd particles, whereas the Pd surface may be fully covered by PDDA causing a mass transport issue at high PDDA loadings. In comparison to PDDA-fuctionalized catalysts, non-functionalized Pd/C (Pd/C-PDDA-0) and commercial Pd/C catalysts show a much lower CO partial current density (<25 mA cm^{-2}) at all potentials (Fig. 2c). The CO FEs for both bare Pd/C catalysts drop quickly below 40% at a potential less than −0.4 V, while the H_2 FEs increase above 80% (Fig. 2b and d). The results clearly suggest that the presence of PDDA in Pd/C catalysts greatly enhances the CO production in CO_2R. Additionally, while formate is a common product for Pd-catalyzed CO_2R in neutral electrolytes, no

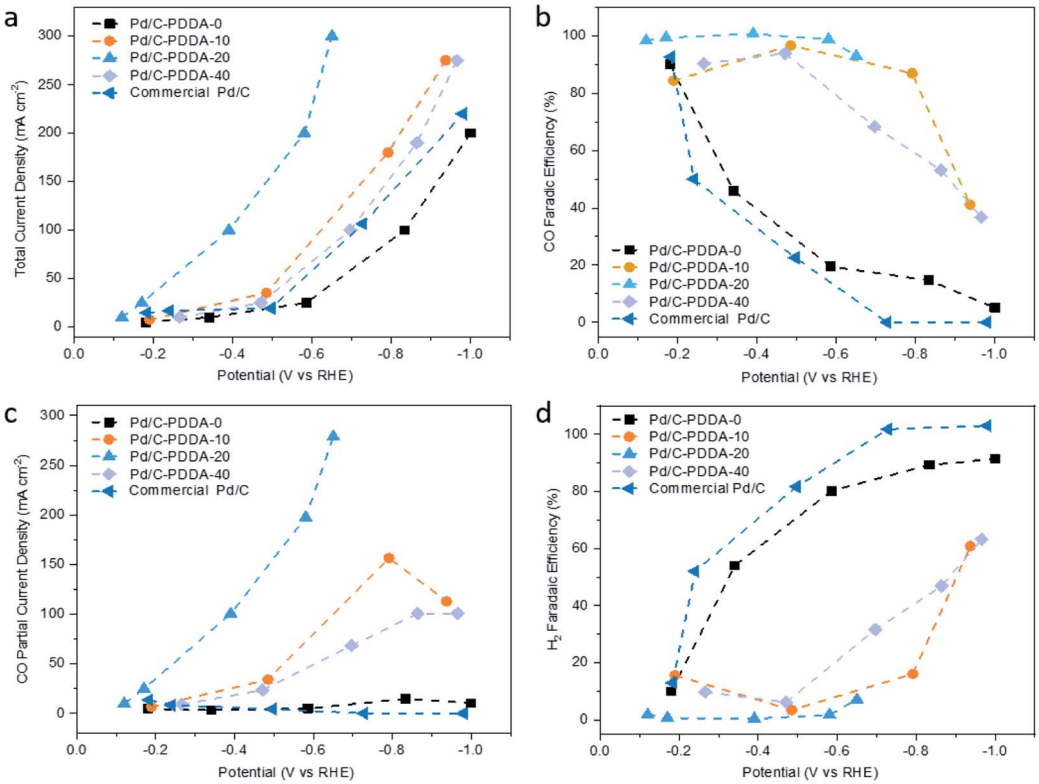

Fig. 2 CO_2R performance of PDDA-functionalized Pd/C catalysts. (a) Total current density, (b) CO faradaic efficiency, (c) CO partial current density, and (d) H_2 faradaic efficiency. Commercial Pd/C catalyst is also shown for comparison.

Published on 07 May 2020. Downloaded by University of Technology Sydney on 08/19/2020 15:34:40.

formate was detected for any PDDA-functionalized Pd/C catalysts under alkaline electrolytes. The low formate formation in CO_2R was also observed for commercial and non-functionalized Pd/C catalysts in alkaline conditions.

To investigate the stability of Pd/C-PDDA-*X* catalysts, a 6 hour CO_2R at a constant potential (−0.4 V) was conducted. The result shows a less than 10% decay of current density together with a high CO FE consistently above 90% and a low H_2 FE below 10%, indicating a stable performance of the Pd/C-PDDA-20. The TEM image of the spent catalyst (Fig. 3a, inset) also confirmed that the morphology of the Pd particles is preserved during the stability test. The XRD measurement of the spent Pd/C-PDDA-20 catalyst showed a similar diffraction pattern to that of the as-synthesized sample (Fig. 3b), indicating the structural integrity of the Pd particles in the PreLONG CO_2R test. For the spent sample, a slight shift of the peaks to low degrees was observed, which is likely due to the formation of the PdH phase in CO_2R, a phenomenon that has been observed in previous Pd-catalyzed CO_2R studies.

To elucidate the role of PDDA in CO_2R, we conducted additional investigations using XPS, CO-TPD-MS, and operando ATR-IR techniques. We suspect that the electron donation from the quaternary ammonium groups in PDDA to Pd nanoparticles leads to an electron-rich Pd surface, which may be responsible for the enhanced CO_2R performance. To verify the hypothesis, XPS analysis was conducted and the results are shown in Fig. 4a. The peaks of Pd 3d XPS spectrum of Pd/C-PDDA-0 centered at 335.1 eV and 340.4 eV are attributed to Pd^0 $3d_{5/2}$ and Pd^0 $3d_{3/2}$,[29] respectively. The Pd 3d peaks for Pd/C-PDDA-20 have a noticeable 0.4–0.5 eV shift compared with Pd/C-PDDA-0 sample. The doublets at higher binding energies belongs to the Pd^{2+}, which could be attributed to the oxide layer on the Pd surface and the oxide layer would be reduced under the electroreduction condition. The blueshift of the Pd binding energy can be attributed to the electron transfer from PDDA to Pd, suggesting a negative shift of the d-band center relative to the Fermi level.[30] According to the d-band center theory proposed by Norskov *et al.*,[31] a negative shift of the d-band center weakens the CO adsorption on Pd surface, resulting in facile desorption of CO intermediate from the Pd surface for the PDDA-functionalized Pd/C catalysts. The XPS results are in good agreement with the high CO selectivity of Pd/C-PDDA-*X* observed in CO_2R.

The CO adsorption strength on Pd/C-PDDA-20 was also measured using CO-TPD-MS. During a CO temperature-programmed desorption measurement, the desorbed substances are first quantified using a TCD detector and then analyzed using MS. CO adsorption on a bare Pd surface is relatively facile, and therefore, the desorption of CO from Pd surface requires a relatively high temperature. As shown in Fig. 4b, a large CO desorption peak centered at 470 °C was observed for Pd/C-PDDA-0, whereas the CO desorption from Pd/C-PDDA-20 has a much smaller peak centered at 443 °C. The result confirms that a much weaker CO binding energy on PDDA-functionalized Pd surface than that of bare Pd surface. Based on both XPS and CO-TPD-MS data, we conclude that the presence of PDDA can effectively weaken the CO adsorption on Pd surface, which, in turn, enhances the CO selectivity of Pd/C-PDDA-20 in CO_2R. The Pd/PDDA properties may change during high temperature CO TPD characterization, and therefore, we also conducted ATR-IR measurements to confirm that CO adsorption on Pd.

To probe CO adsorption on Pd/C catalysts under applied potentials, operando ATR-FTIR experiments were conducted under a constant CO gas flow for both Pd/C-PDDA-20 and Pd/C-PDDA-0 catalysts. For Pd/C-PDDA-0, the peaks at 2000 cm^{-1} and 1895 cm^{-1} (Fig. 5a) can be assigned to bridge-bonded CO* species (CO_B) and linear-bonded CO* species (CO_L), respectively.[22] At more negative potentials, both peaks shift to low wavenumbers, indicating a slower vibration frequency of surface bounded CO which is due to Stark tuning effect caused by a stronger electric field and a higher CO binding strength on the Pd surface. This observation is in good agreement with previous studies on metal-catalyzed CO_2R.[32] Moreover, the wavenumbers of both CO_L and CO_B peaks for Pd/C-PDDA-20 are

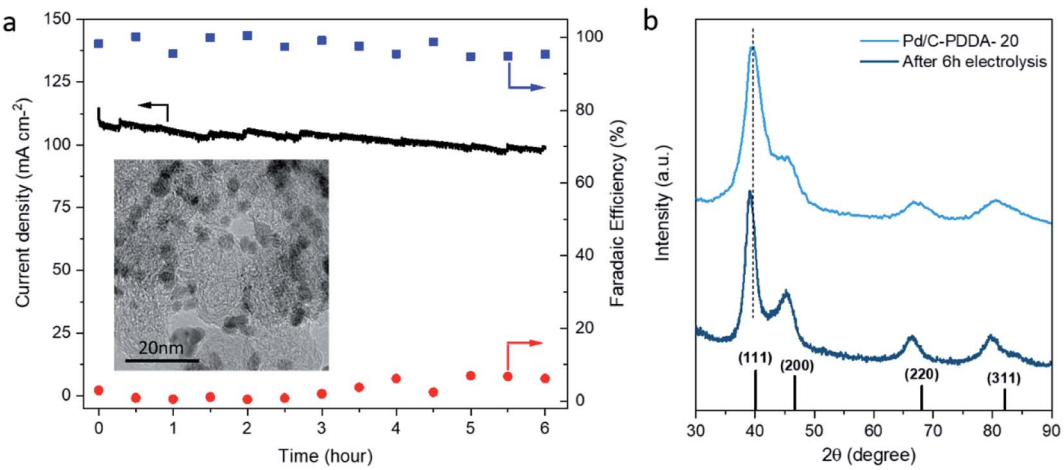

Fig. 3 (a) CO_2R stability test of Pd/C-PDDA-20 at a constant potential of −0.4 V for 6 hours. Inset is a TEM image of the spent catalyst. (b) XRD patterns for Pd/C-PDDA-20 before and after the 6 hour stability test.

 This journal is © The Royal Society of Chemistry 2020

Published on 07 May 2020. Downloaded by University of Technology Sydney on 08/19/2020 15:34:40.

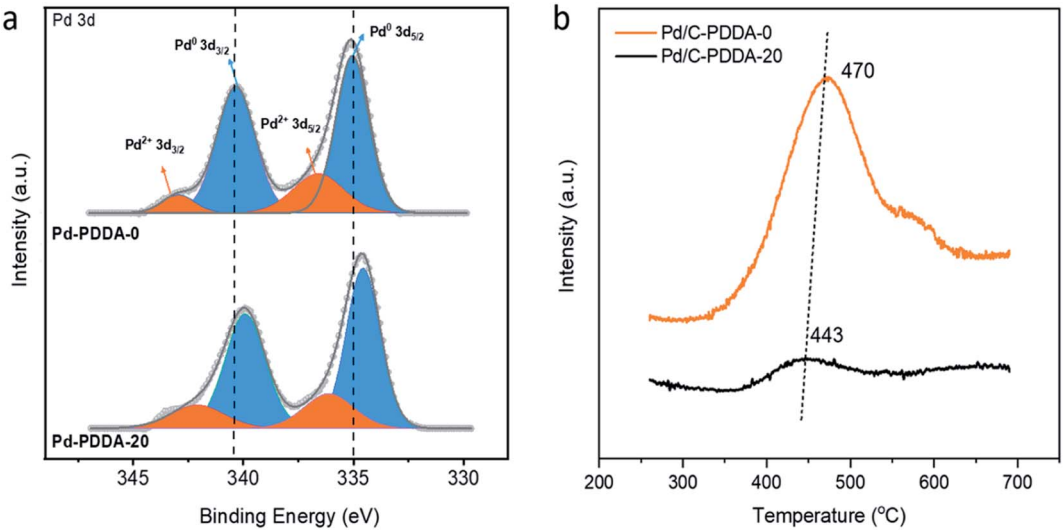

Fig. 4 (a) XPS Pd 3d spectra and (b) CO-TPD-MS data for Pd/C-PDDA-0 and Pd/C-PDDA-20.

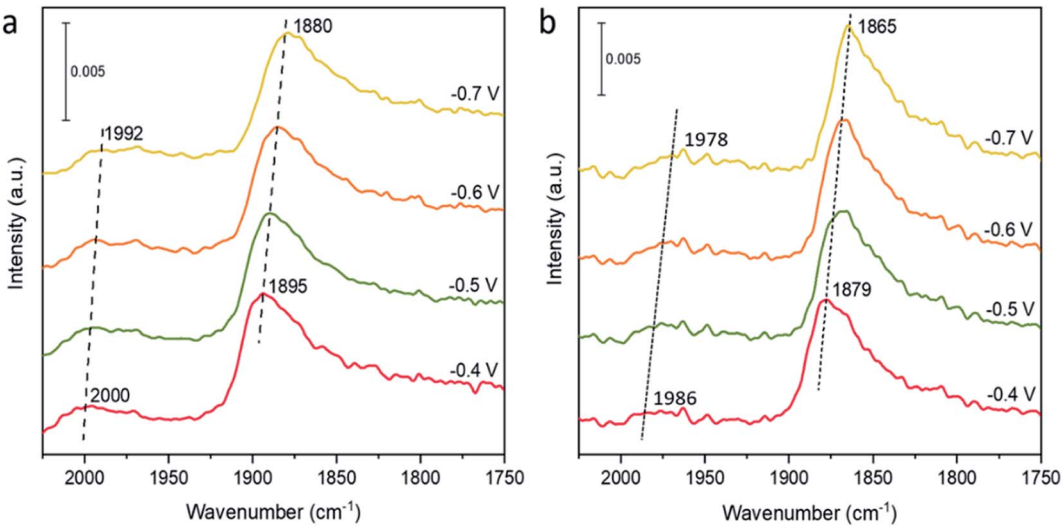

Fig. 5 Operando ATR-IR spectra for (a) Pd/C-PDDA-20 and (b) Pd/C-PDDA-0 at various applied potentials.

significantly higher than those of Pd/C-PDDA-0 (Fig. 5b), indicating a higher vibration frequency for Pd/C-PDDA-20, and thus a weaker CO binding energy on Pd. The ATR-FTIR results further confirm that the introduction of PDDA to Pd/C catalyst effectively reduces its CO binding energy on Pd, which leads to the enhanced CO selectivity of Pd/C-PDDA-*X* in CO_2R.

4. Conclusion

In summary, we demonstrated that PDDA-functionalized Pd/C catalysts can achieve a maximum current density of 300 mA cm^{-2} with a 93% CO FE at −0.65 V. The origin of the enhanced properties of PDDA-functionalized Pd/C catalysts is explored using XPS, CO-TPD-MS, and operando ATR-FTIR. The results confirmed that the presence of PDDA significantly reduces CO binding strength on the Pd surface, which facilitates the desorption of CO intermediate in CO_2R, and consequently, a high CO FE was obtained. This work shows that the introduction of PDDA functionalization on metal catalyst surfaces can be an effective approach to alter the CO binding energy of metal catalysts, resulting in an improved CO_2 reduction performance.

Conflicts of interest

There are no conflicts to declare.

Acknowledgements

R. X. and F. J. would like to acknowledge the financial support from the China Scholarship Council (CSC) and the National Science Foundation (CBET Award#: 1803200). S. Z. and X. B. M.

Published on 07 May 2020. Downloaded by University of Technology Sydney on 08/19/2020 15:34:40.

gratefully acknowledge support from Tianjin Key Science and Technology Project (19ZXNCGX00030 and 18ZXJMTG00180).

References

1 S. Zhu, Q. Wang, X. Qin, M. Gu, R. Tao, B. P. Lee, L. Zhang, Y. Yao, T. Li and M. Shao, *Adv. Energy Mater.*, 2018, **8**, 1802238.
2 J. Fu, W. Zhu, Y. Chen, Z. Yin, Y. Li, J. Liu, H. Zhang, J. J. Zhu and S. Sun, *Angew. Chem., Int. Ed.*, 2019, **58**, 14100–14103.
3 Z. Cao, D. Kim, D. Hong, Y. Yu, J. Xu, S. Lin, X. Wen, E. M. Nichols, K. Jeong, J. A. Reimer, P. Yang and C. J. Chang, *J. Am. Chem. Soc.*, 2016, **138**, 8120–8125.
4 S. Liu, C. Sun, J. Xiao and J.-L. Luo, *ACS Catal.*, 2020, 3158–3163, DOI: 10.1021/acscatal.9b03883.
5 Q. Lu, J. Rosen, Y. Zhou, G. S. Hutchings, Y. C. Kimmel, J. G. Chen and F. Jiao, *Nat. Commun.*, 2014, **5**, 1–6.
6 M. Ma, B. J. Trześniewski, J. Xie and W. A. Smith, *Angew. Chem., Int. Ed.*, 2016, **55**, 9748–9752.
7 J. Rosen, G. S. Hutchings, Q. Lu, R. V. Forest, A. Moore and F. Jiao, *ACS Catal.*, 2015, **5**, 4586–4591.
8 D. H. Won, H. Shin, J. Koh, J. Chung, H. S. Lee, H. Kim and S. I. Woo, *Angew. Chem., Int. Ed.*, 2016, **55**, 9297–9300.
9 W. Sheng, S. Kattel, S. Yao, B. Yan, Z. Liang, C. J. Hawxhurst, Q. Wu and J. G. Chen, *Energy Environ. Sci.*, 2017, **10**, 1180–1185.
10 J. Wang, S. Kattel, C. J. Hawxhurst, J. H. Lee, B. M. Tackett, K. Chang, N. Rui, C. J. Liu and J. G. Chen, *Angew. Chem., Int. Ed.*, 2019, **58**, 6271–6275.
11 X. Yuan, L. Zhang, L. Li, H. Dong, S. Chen, W. Zhu, C. Hu, W. Deng, Z.-J. Zhao and J. Gong, *J. Am. Chem. Soc.*, 2019, **141**, 4791–4794.
12 Q. He, J. H. Lee, D. Liu, Y. Liu, Z. Lin, Z. Xie, S. Hwang, S. Kattel, L. Song and J. G. Chen, *Adv. Funct. Mater.*, 2020, 2000407.
13 D. Gao, H. Zhou, F. Cai, J. Wang, G. Wang and X. Bao, *ACS Catal.*, 2018, **8**, 1510–1519.
14 D. Gao, H. Zhou, F. Cai, D. Wang, Y. Hu, B. Jiang, W.-B. Cai, X. Chen, R. Si and F. Yang, *Nano Res.*, 2017, **10**, 2181–2191.
15 D. Gao, H. Zhou, J. Wang, S. Miao, F. Yang, G. Wang, J. Wang and X. Bao, *J. Am. Chem. Soc.*, 2015, **137**, 4288–4291.
16 H. Huang, H. Jia, Z. Liu, P. Gao, J. Zhao, Z. Luo, J. Yang and J. Zeng, *Angew. Chem., Int. Ed.*, 2017, **56**, 3594–3598.
17 Q. Li, J. Fu, W. Zhu, Z. Chen, B. Shen, L. Wu, Z. Xi, T. Wang, G. Lu and J.-j. Zhu, *J. Am. Chem. Soc.*, 2017, **139**, 4290–4293.
18 W. Zhu, S. Kattel, F. Jiao and J. G. Chen, *Adv. Energy Mater.*, 2019, **9**, 1802840.
19 H. Dong, L. Zhang, P. Yang, X. Chang, W. Zhu, X. Ren, Z.-J. Zhao and J. Gong, *Chem. Eng. Sci.*, 2019, **194**, 29–35.
20 J. H. Lee, S. Kattel, Z. Jiang, Z. Xie, S. Yao, B. M. Tackett, W. Xu, N. S. Marinkovic and J. G. Chen, *Nat. Commun.*, 2019, **10**, 1–8.
21 Y. Mun, S. Lee, A. Cho, S. Kim, J. W. Han and J. Lee, *Appl. Catal., B*, 2019, **246**, 82–88.
22 S. Zhu, X. Qin, Q. Wang, T. Li, R. Tao, M. Gu and M. Shao, *J. Mater. Chem. A*, 2019, **7**, 16954–16961.
23 F. W. Li, A. Thevenon, A. Rosas-Hernández, Z. Y. Wang, Y. L. Li, C. M. Gabardo, A. Ozden, C. T. Dinh, J. Li, Y. H. Wang, J. P. Edwards, Y. Xu, C. McCallum, L. Z. Tao, Z. Q. Liang, M. C. Luo, X. Wang, H. H. Li, C. P. O'Brien, C. S. Tan, D. H. Nam, R. Quintero-Bermudez, T. T. Zhuang, Y. G. C. Li, Z. J. Han, R. D. Britt, D. Sinton, T. Agapie, J. C. Peters and E. H. Sargent, *Nature*, 2020, **577**, 509–513.
24 S. Zhang, Y. Shao, G. Yin and Y. Lin, *J. Mater. Chem.*, 2009, **19**, 7995–8001.
25 M. Jouny, W. Luc and F. Jiao, *Nat. Catal.*, 2018, **1**, 748–755.
26 J. Wu, S. Ma, J. Sun, J. I. Gold, C. Tiwary, B. Kim, L. Zhu, N. Chopra, I. N. Odeh and R. Vajtai, *Nat. Commun.*, 2016, **7**, 1–6.
27 J. J. Lv, M. Jouny, W. Luc, W. Zhu, J. J. Zhu and F. Jiao, *Adv. Mater.*, 2018, **30**, 1803111.
28 W. Luc, X. B. Fu, J. J. Shi, J. J. Lv, M. Jouny, B. H. Ko, Y. B. Xu, Q. Tu, X. B. Hu, J. S. Wu, Q. Yue, Y. Y. Liu, F. Jiao and Y. J. Kang, *Nat. Catal.*, 2019, **2**, 423–430.
29 L. Jiao, F. Li, X. Li, R. Ren, J. Li, X. Zhou, J. Jin and R. Li, *Nanoscale*, 2015, **7**, 18441–18445.
30 H. Tsunoyama, N. Ichikuni, H. Sakurai and T. Tsukuda, *J. Am. Chem. Soc.*, 2009, **131**, 7086–7093.
31 M. Mavrikakis, B. Hammer and J. K. Norskov, *Phys. Rev. Lett.*, 1998, **81**, 2819–2822.
32 J. Heyes, M. Dunwell and B. Xu, *J. Phys. Chem. C*, 2016, **120**, 17334–17341.

 This journal is © The Royal Society of Chemistry 2020